DALTON
FULL PAPER

Structural distortions in homoleptic $(RE)_4A$ (E = O, S, Se; A = C, Si, Ge, Sn): implications for the CVD of tin sulfides

Giampaolo Barone,†[a] Thomas G. Hibbert,[a] Mary F. Mahon,[a] Kieran C. Molloy,*[a] Ivan P. Parkin,[b] Louise S. Price[b] and Ioan Silaghi-Dumitrescu[c]

[a] *Department of Chemistry, University of Bath, Claverton Down, Bath, UK BA2 7AY*
[b] *Department of Chemistry, University College London, 20 Gordon Street, London, UK WC1H 0AJ*
[c] *Department of Chemistry, Babes-Bolyai University, RO-3400, Cluj-Napoca, Romania*

Received 19th December 2000, Accepted 8th October 2001
First published as an Advance Article on the web 9th November 2001

The structures of $Sn(SBu^t)_4$ and $Sn(SCy)_4$ have been determined and adopt S_4 and D_2 conformations respectively; the anion $[(PhS)Sn_3]^-$, as its Ph_4P^+ salt, has a structure approaching C_s symmetry. In all three compounds, there are large variations in the ∠S–Sn–S within the same molecule, which have been rationalised in terms of the C–S–Sn–S–C conformations. For $Sn(SR)_4$, the ∠S–Sn–S increases as the conformations change from *trans*, *trans* to *trans*, *gauche* and *gauche*, *gauche*, as the number of eclipsed lone pairs decreases and this rationale is shown to be applicable to a variety of $A(ER)_4$ (A = C, Si, Ge, Sn; E = O, S, Se) and related [$Mo(SR)_4$, $Ga(SR)_4^-$] systems. AM1 calculations have been used to model the ∠S–Sn–S magnitudes and also provide insights into the decomposition mechanisms of these and related species which are relevant to chemical vapour deposition processes.

Introduction

We have been interested for some time in precursors for the deposition of the family of tin sulfides (SnS_2, Sn_2S_3, SnS), an important class of semiconductor materials.[1–4] In an effort to find "single-source" routes to thin films of these sulfides, we have focussed attention on the homoleptic thiolates $(RS)_4Sn$, as these seem ideally constructed to produce the desired materials. While we have been able to introduce sufficient volatility into the precursors (R = CF_3CH_2) for deposition at atmospheric pressure (APCVD—atmospheric pressure chemical vapour deposition),[5] other homologues (*e.g.* R = Ph) require nebulisation (AACVD—aerosol-assisted chemical vapour deposition).[6] Of considerable surprise in these studies was the failure to deposit tin sulfide films from the precursors *in the absence of H_2S gas*. Indeed, when H_2S is absent we deposit films of the metastable oxide, Sn_3O_4, instead.[5] In an attempt to rationalise these findings, we have focussed our attention on the structures of the precursors and the implications of these structures for their decomposition pathway.

We have previously reported the structures of $(PhS)_4Sn$[6] and $[CF_3(CF_2)_5CH_2CH_2S]_4Sn$,[5] the first structurally characterised examples of tetrahedral, homoleptic tin(IV) thiolates. The structures of both $[MeS(Ph)C{=}C(Ph)S]_4Sn$,[7] $(PyS)_4Sn$[8] and $(3\text{-}Me_3SiC_5H_3NS\text{-}2)_4Sn$[9] are known, but weak intramolecular chelation hides the underlying structural trends. Despite their symmetric, homoleptic nature, the structures of $(RS)_4Sn$ are, in fact, remarkably distorted, with ∠S–Sn–S in the range 102.8–114.9°. This is in keeping with known distortions in analogous organic systems $[(RO)_4C]$, which have been the subject of much debate.[10] The anomeric effect has figured predominantly in this argument and has been used to explain the preferred *gauche* conformation for dimethoxymethane (**1a**), while the eclipsed lone pair–lone pair (lp–lp) interactions are believed to strongly disfavour the *trans* conformation (**1b**). Several authors have noted the importance of lp–lp repulsions in determining conformational preference, although these conflict with calculations which show that the optimised ∠O–C–O in dimethoxymethane is at a minimum (102°) in **1b**.[11] The authors of the latter work concluded that lone pairs effects are directionally *invisible* and that bond–bond interactions dominate. More recently, Gillespie and Robinson have championed a ligand close-packing approach (LCP)[12] which, for species with significant ionic character to the bonds [including $A(OH)_4$, A = Be, B, C], rationalises molecular geometry as being dictated by the close approach of the non-bonding, partially charged ligands (*i.e.* δ + /− of significant magnitude) about the central atom. In this model, it is the $E(\delta-)\cdots E(\delta-)$ repulsions (**1c**) which determine A–E bond lengths and conformations, and the non-spherical nature of the electron density around the atom E in $A(ER)_4$ (by virtue of the presence of two lone electron pairs) means that the effective atomic radius varies with direction. Moreover, the fact that E has a smaller radius on the side of the lone pairs allows atoms to approach closer when these lone pairs are oriented toward each other.[13] Paradoxically, in the light of other analyses focussing on lp–lp repulsions, this argument says that the narrow ∠O–C–O in **1b** is precisely due to the lack of repulsive interactions between lone pairs. However, while this approach could be used to support the calculated bond angle diminution in **1b**, it has so far only been applied to situations which can be described as *nearly ionic*.

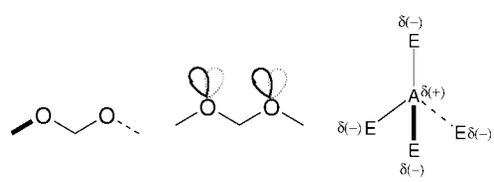

(**1a**) (**1b**) (**1c**)

In this paper, we analyse the conformational preferences for a wide range of $A(ER)_4$ systems (A = C, Si, Ge, Sn; E = O, S, Se), based upon available crystallographic data, and interpret these findings in the light of current bonding theories, the results of which have significant implications for our CVD experiments.

† On leave from Departimento di Chimica Inorganica, Università di Palermo, Via Arcirafi 26–28, Palermo 90123, Italy.

DOI: 10.1039/b010157p

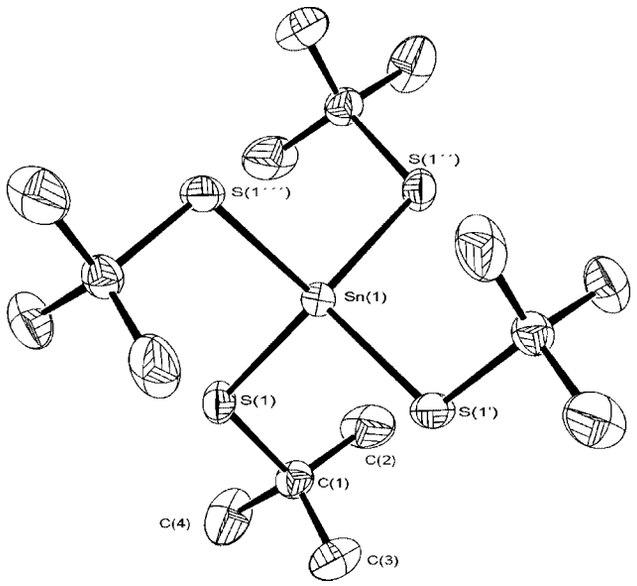

Fig. 1 The asymmetric unit of $Sn(SBu^t)_4$. Primed atoms are related to their unprimed counterparts by $2 - x, -y, z$ (′), $2 - y, x, 2 - z$ (″), $y, 2 - x, 2 - z$ (‴); thermal ellipsoids are at the 30% probability. Selected metric data: Sn(1)–S(1) 2.397(2) Å; S(1)–Sn(1)–S(1′) 117.17(10), S(1)–Sn(1)–S(1″) 105.77(5), C(1)–S(1)–Sn(1) 110.1(2)°.

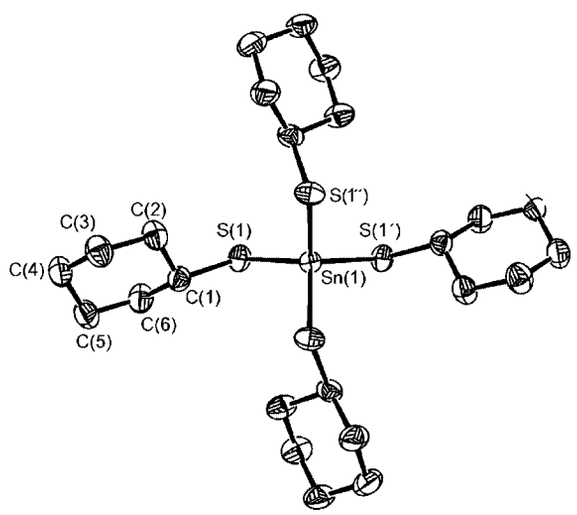

Fig. 2 The asymmetric unit of $Sn(SCy)_4$. Primed and doubly primed atoms are related to their unprimed counterparts by $y, 1/2 - x, 1/2 - z$ and $1/2 - x, 1/2 - y, z$, respectively; thermal ellipsoids are at the 30% probability. Selected metric data: Sn(1)–S(1) 2.382(1) Å; S(1)–Sn(1)–S(1′) 114.82(3), S(1)–Sn(1)–S(1″) 99.23(5)°.

Results and discussion

Synthesis and crystallography

$Sn(SBu^t)_4$ was prepared from $SnCl_4$ and $NaSBu^t$ in toluene following established methodologies.[14–16] $Sn(SC_6H_{11})_4$ was also prepared as described elsewhere[17] from $SnCl_4$ and $C_6H_{11}SLi$ and isolated as colourless crystals. $[Ph_4P][Sn(SPh)_3]$ was prepared by the method of Dean *et al.* from $SnCl_2$ and NaSPh in the presence of $[Ph_4P]Br$.[18] The latter compound is stable in air in the solid state, the Mössbauer spectrum showing no increase in Sn(IV) content after 1 week; aerobic oxidation is, however, rapid when the compound is in solution.

The asymmetric units of the three compounds are shown in Figs. 1–3, respectively, along with selected metrical data. $Sn(SBu^t)_4$ is tetrahedral at tin with Sn–S = 2.397(2) Å. The thiolate groups are arranged about the metal in a conformation which has S_4 symmetry, with the metal located on a crystallographically-imposed −4 site. Of the six ∠S–Sn–S, two are

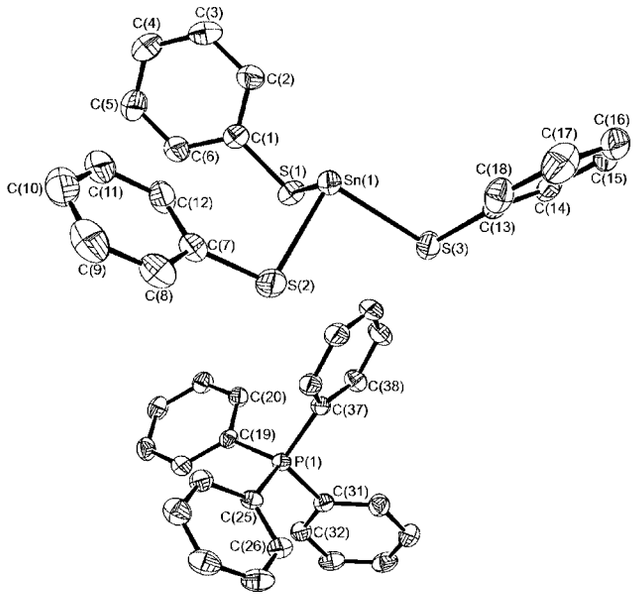

Fig. 3 The asymmetric unit of $[Ph_4P][(PhS)_3Sn]$. Thermal ellipsoids are at the 30% probability. Selected metric data: Sn(1)–S(1) 2.5561(8), Sn(1)–S(2) 2.5367(9), Sn(1)–S(3) 2.5336(8) Å; S(2)–Sn(1)–S(1) 96.87(3), S(3)–Sn(1)–S(1) 89.57(3), S(3)–Sn(1)–S(2) 90.88(3), C(1)–S(1)–Sn(1) 99.14(9), C(7)–S(2)–Sn(1) 98.38(10), C(13)–S(3)–Sn(1) 101.37(9)°.

opened significantly [117.17(10)°] while four are reduced from the ideal tetrahedral value [105.77(5)°] in an arrangement which resembles the structure of $(PhS)_4Sn$.[6] In $Sn(SCy)_4$ (Fig. 2), all Sn–S bond lengths are 2.382(1) Å, whereas the S–Sn–S angles vary dramatically between 99.23(5) and 114.82(3)°. Unlike $Sn(SPh)_4$ and $Sn(SBu^t)_4$, $Sn(SCy)_4$ adopts a D_2 conformation with two narrow and four wide ∠S–Sn–S. Deviations from the tetrahedral ideal similar to those described for these two tin thiolates are evident in the solid state structures of $(PhS)_4C$[19] and $(PhS)_4Si$[20] showing that this effect is common to other analogous group 14 thiolates, and the distorted tetrahedral structures of $(^tBuO)_4Sn$,[21] $(PhO)_4C$,[10] $(PhSe)_4Sn$[22] and $(PhSe)_4Ge$[23] show that homoleptic alkoxide and selenate ligands act in similar manner. "Packing factors" are often invoked to explain these structural distortions, but in a more in-depth analysis, the deviation from tetrahedral geometry in $(PhO)_4C$ has been attributed to a cumulative anomeric effect.[10] This explanation appears less convincing when applied to compounds with much longer A–E (A = C–Sn; E = O–Se) bonds and which incorporate heavier group 16 elements, for which the anomeric effect is believed to be negligible.

The structure of the thiolate anion $[(PhS)_3Sn]^-$, as its tetraphenylphosphonium salt, closely mirrors the analogous tetraphenylarsonium derivative, whose structure has also been reported,[18] despite the change of counterion (Fig. 3). The geometry can be described as trigonal pyramidal, *i.e.* tetrahedral with one site occupied by a stereochemically active lone electron pair. The Sn–S bonds [2.5336(8), 2.5367(9), 2.5561(8) Å] are longer than in the neutral Sn(IV) thiolates (*vide supra*). The S–Sn–S bond angles are not regular, with one angle [96.87(3)°] significantly larger than the other two [89.57(3), 90.88(3)°]. The overall conformations of the three Sn–SPh units lead to the anion approaching idealised C_s symmetry. The related homoleptic Sn(IV) anion $[(PhS)_5Sn]^-$ is also reported to be distinctly distorted from a trigonal bipyramidal structure,[24] though a full account of this structure does not appear to have been published.

Conformational analysis

The structural data for $A(ER)_4$ are collected in Tables 1–3 for E = O, S and Se, respectively. The structures adopted are rarely of crystallographic high symmetry, but can largely be divided between the idealised point groups S_4 (**2a**) and D_2 (**2b**) (D_{2d} if

Table 1 Structural data for $A(OR)_4$ (A = C, Si, Ge, Sn) †

	CODE	$(PhO)_4C$ KEVFOG		$(3,5\text{-}Me_2C_6H_3O)_4C$ KEVFUM		$(PhCH_2O)_4C$ VALSIK		$(^iPrO)_4Si$ RATPUX	$(^tBuO)_4Sn$ VISKIR
Conformation	Symmetry	D_2	D_2	D_2	D_2	S_4	S_4	S_4	S_4
	A–O	1.390 (2) 1.396 (2)	1.389 (2) 1.391 (2)	1.382, 1.397 1.405, 1.419	1.361, 1.392 1.394, 1.417	1.391, 1.393 1.394, 1.396	1.392, 1.393 1.396, 1.404	1.615 (4)	1.947 (2) 1.949 (2)
	O···O(short)	2.137, 2.168	2.149, 2.151	2.161, 2.187	2.120, 2.165	2.245, 2.250 2.251, 2.253	2.243, 2.246 2.257, 2.262	2.594(4)	3.105 (2) 3.140 (2)
	O···O(long)	2.331 (2) 2.336 (2)	2.326 (2) 2.327 (2)	2.291, 2.330 2.349, 2.351	2.303, 2.321 2.342, 2.366	2.322, 2.332	2.333, 2.338	2.723 (2)	3.285, 3.302
t, *t* (*ap*, *ap*)	∠O–A–O	100.4	101.3	101.0	99.1				
	∠C–O–A–O	171.6, 171.6	−166.8, −166.8	172.1, 174.2	177.3, 177.1				
	∠O–A–O	101.9	101.4	102.6	102.4				
	∠C–O–A–O	−174.7, −174.7	173.6, 173.6	−170.5, −168.8	−173.0, −172.0				
t, *g* (*ap*, *sc*)	∠O–A–O					107.5	106.9	106.8 (4)	105.7 (2)
	∠C–O–A–O					176.7, 53.8	177.2, 52.7	−162.7, 39.3	166.3, −42.4
	∠O–A–O					107.6	107.0		107.4 (2)
	∠C–O–A–O					179.3, 65.0	−176.3, 63.3		−165.7, 42.1
	∠O–A–O					107.7	108.0		
	∠C–O–A–O					176.4, −58.7	175.9, −54.5		
	∠O–A–O					107.8	108.1		
	∠C–O–A–O					−172.2, −61.3	−173.4, −61.0		
g, *g* (*sc*, *sc*)	∠O–A–O	113.6 (2)	113.6 (2)	111.1	112.9	112.9	112.9	114.9 (2)	115.9 (2)
	∠C–O–A–O	−66.4, −51.7	−64.0, −44.5	66.0, 48.0	65.6, 55.2	−65.0, −53.6	−66.0, −55.4	−79.0, −79.0	76.4, 76.4
	∠O–A–O	113.9 (2)	113.7 (2)	111.2	113.4	113.5	114.1		
	∠C–O–A–O	49.7, 62.5	70.8, 51.2	66.0, 51.6	−60.7, −51.1	60.1, 57.7	64.2, 57.9		
	∠O–A–S			115.1	114.8				
	∠C–O–A–O			−68.0, −48.1	−56.8, −46.8				
	∠O–A–O			116.5	114.9				
	∠C–O–A–O			−65.5, −48.8	61.5, 61.9				

[a] Numbers in parentheses refer to the number of occurrences of a given datum; *e.g.* all four Si–O bonds have length 1.615 Å in $(^iPrO)_4Si$.

Table 2 Structural data for $A(SR)_4$ (A = C, Si, Ge, Sn) ‡

Conformation	CODE Symmetry	$(MeS)_4C$ TMOSCA S_4	$(PhS)_4C$ TPHOTC S_4	$(PhS)_4Si$ JEWJEA S_4	$(p\text{-TolS})_4Ge$ HEWGAR S_4	$(PhS)_4Sn$[6] S_4	$(^tBuS)_4Sn$ This work S_4	$(CyS)_4Sn$ This work D_2
	A–S	1.819 (4)	1.810, 1.828 1.832, 1.835	2.123 (2) 2.129 (2)	2.211, 2.216 2.221 (2)	2.379 (2) 2.401 (2)	2.397 (4)	2.382 (4)
	S···S(short)	2.964 (4)	2.868, 2.919 2.944, 2.957	3.375 (2) 3.414 (2)	3.519, 3.548 3.555, 3.566	3.861 (2) 3.818 (2)	3.823 (4)	3.629 (2)
	S···S(long)	2.981 (2)	3.087, 3.108	3.618, 3.623	3.741, 3.783	4.010, 4.040	4.091 (2)	4.014 (4)
t, *t* (*ap*, *ap*)	∠S–A–S ∠C–S–A–S							99.2 (2) 164.8, 164.8
t, *g* (*ap*, *sc*)	∠S–A–S ∠C–S–A–S ∠S–A–S ∠C–S–A–S ∠S–A–S ∠C–S–A–S ∠S–A–S ∠C–S–A–S	109.2 (4) 177.7, 61.9	103.9 177.8, −57.1 105.5 179.2, 66.3 107.0 −170.7, −44.4 108.7 −171.6, 54.8	105.1 (2) 169.3, −49.5 106.8 (2) −174.3, 44.8	105.0 177.4, 59.8 106.2 168.9, 55.4 106.7 173.7, 42.9 107.1 −174.6, −63.0	106.0 (2) −167.1, 49.7 107.8 (2) 173.2, −43.9	105.8 (4) 177.2, −52.2	
g, *g* (*sc*, *sc*)	∠S–A–S ∠C–S–A–S ∠S–A–S ∠C–S–A–S	110.1 (2) 57.9, 57.9	115.0 72.4, 61.6 117.0 −48.6, −48.6	116.6 68.6, 68.6 116.9 −72.5, −72.5	114.8 75.6, −56.4 117.4 63.8, 54.7	114.6 (1) 74.0, 74.0 114.9 (1) −69.0, −69.0	117.2 (2) −65.3, −65.3	114.8 (4) 72.3, 41.8

[a] Numbers in parentheses refer to the number of occurrences of a given datum; *e.g.* all four Sn–S bonds have length 2.397 Å in $(^tBuS)_4Sn$.

Table 3 Structural data for $A(SeR)_4$ (A = Si, Ge, Sn)

Conformation	CODE Symmetry	$(PhSe)_4Si$ JEWJIE S_4	$(PhSe)_4Ge$ JAFWES S_4	$(PhSe)_4Sn$ BEMBUQ S_4	$(MesSe)_4Ge$ HEWGEV C_2	$(PhSe)_4Sn$ BEMBUQ01 C_2
	A–Se	2.272 (2) 2.274 (2)	2.344 (2) 2.347 (2)	2.513 (4)	2.365, 2.368 2.378, 2.386	2.478, 2.488 2.499, 2.505
	Se···Se(short)	3.618 (2) 3.647 (2)	3.747 (2) 3.776 (2)	4.032 (2) 4.047 (2)	3.735, 3.781 3.853, 3.918	4.041, 4.043 4.046, 4.049
	Se···Se(long)	3.857, 3.872	3.954, 3.974	4.212, 4.246	3.946, 4.011	4.098, 4.144
t, *g* (*ap*, *sc*)[b]	∠Se–A–Se ∠C–Se–A–Se ∠Se–A–Se ∠C–Se–A–Se ∠Se–A–Se ∠C–Se–A–Se ∠Se–A–Se ∠C–Se–A–Se	105.5 (2) 170.3, −50.3 106.7 (2) −174.5, 45.5	106.0 (2) 169.6, −51.3 107.2 (2) −174.6, 45.4	106.7 (2) −168.7, 52.9 107.3 (2) 175.2, −44.6	103.6 146.3, −6.0 105.7 161.3, 2.3 108.4 121.1, 114.3 110.7 −130.2, 44.1	108.0 174.9, 9.1 108.0 −68.1, −63.3 108.8 171.7, 7.4 109.0 130.2, 130.2
g, *g* (*sc*, *sc*)[b]	∠Se–A–Se ∠C–Se–A–Se ∠Se–A–Se ∠C–Se–A–Se	116.2 −71.7, −71.7 116.7 67.9, 67.9	115.0 −72.2, −72.2 115.7 67.4, 67.4	113.8 73.2, 73.2 115.3 −66.1, −66.1	113.0 −124.7, 29.2 115.4 −92.6, −73.1	110.7 −130.2, 44.1 112.4 109.1, 50.9

[a] Numbers in parentheses refer to the number of occurrences of a given datum; *e.g.* all four Sn–Se bonds have length 2.513 Å in $(PhSe)_4Sn$ (BEMBUQ). [b] Does not apply to compounds of C_2 symmetry.

the six dihedrals fall into two groups of four and two, within which the angles which are identical within each group, *e.g.* 2 × 180°, 4 × 60°). On the basis of an additive approach to the anomeric effect, the S_4 conformation has been variously calculated to be *ca.* 6–25 kJ mol^{-1} more stable than the D_{2d} form.[10,25] The flatness of the potential energy surface is further endorsed by the adoption of a third conformation (**2c**; C_2) by two compounds, $(2,4,6\text{-}Me_3C_6H_2Se)_4Ge$[26] and $(PhSe)_4Sn$.[22] While the conformation of the former might be due to the presence of intermolecular Se···Se interactions and/or the steric demands of the $2,4,6\text{-}Me_3C_6H_2$ ligands, the latter exists in both C_2 and S_4 polymorphic forms, uninfluenced by such factors.

In each of the three conformations, the ∠E–A–E deviate from 109° and, as a result, the E···E contacts are variable. In the S_4 conformer, there are 4 short and 2 long E···E interactions, while the situation is reversed when the symmetry changes to D_2. In general, D_2 symmetry leads to greater E···E

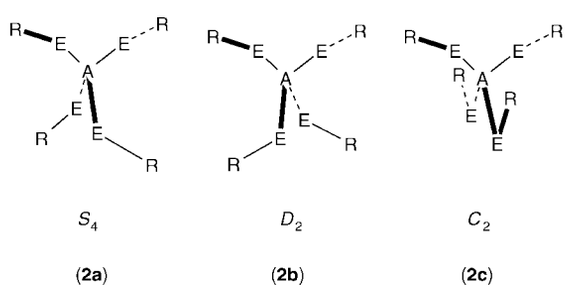

(**2a**) (**2b**) (**2c**)

Table 4 Averaged structural data for $(ER)_4A$ and $[A(ER)_3]^-$ (A = Ge, Sn; E = S, Se)

	$C(OR)_4$			$Si(OR)_4$	$Sn(OR)_4$				
	D_2	S_4	All	S_4	S_4				
E···E(short)	2.15(2)	2.25(1)	2.20(5)	2.59	3.13(2)				
E···E(long)	2.33(2)	2.33(1)	2.33(2)	2.72	3.29(1)				
Δ(E···E)	0.18	0.08	0.13	0.13	0.16				
	$C(SR)_4$	$Si(SR)_4$	$Ge(SR)_4$	$[(PhS)_3Ge]^-$	$Sn(SR)_4$			$[(PhS)_3Sn]^-$	
	S_4	S_4	S_4	C_s	D_2	S_4	All	C_s	
E···E(short)	2.94(3)	3.39(2)	3.55(2)	3.32(11)	3.63	3.83(2)	3.79(9)	3.60(1)	
E···E(long)	3.04(6)	3.62(4)	3.76(3)	3.69	4.01	4.06(4)	4.04(4)	3.81(1)	
Δ(E···E)	0.10	0.23	0.21	0.37	0.38	0.23	0.25	0.21	
	$Si(SeR)_4$	$Ge(SeR)_4$			$[(PhSe)_3Ge]^-$	$Sn(SeR)_4$			$[(PhSe)_3Sn]^-$
	S_4	C_2	S_4	All	C_s	C_2	S_4	All	C_s
E···E(short)	3.63(2)	3.82(8)	3.76(2)	3.79(6)	3.50(1)	4.05(1)	4.04(1)	4.04(1)	3.73(1)
E···E(long)	3.86(1)	3.98(5)	3.96(1)	3.97(3)	3.81	4.12(3)	4.23(2)	4.18(7)	3.99
Δ(E···E)	0.23	0.16	0.20	0.18	0.31	0.07	0.21	0.14	0.26

[a] Data from Tables 1–3 averaged; esds in parentheses.

Table 5 Structural data for $[A(ER)_3]^-$ (A = Ge, Sn; E = S, Se)

	CODE Symmetry	$[(PhS)_3Ge]^-$ [a] HEWFEU C_s	$[(PhS)_3Sn]^-$ [b] This work C_s	$[(PhS)_3Sn]^-$ [c] DARYAW C_s	$[(PhSe)_3Ge]^-$ [b] HEWFIV C_s	$[(PhSe)_3Sn]^-$ [c] DARVEA C_s
	A–E	2.321 2.367, 2.374	2.534, 2.537 2.556	2.532 (2) [d] 2.552	2.469, 2.479 2.501	2.649, 2.650 2.670
	E···E(short)	3.245, 3.400	3.585, 3.612	3.592, 3.598	3.490, 3.499	3.720, 3.738
	E···E(long)	3.691	3.810	3.801	3.812	3.993
3b	∠E–A–E	87.6	89.6	89.9	89.2	88.7
	∠C–E–A–E	−168.7, 157.6	−163.4, 141.3	−164.1, −164.1	−165.0, 141.5	−165.5, 141.3
	∠E–A–E	92.8	90.0	90.6	90.0	89.7
	∠C–E–A–E	−177.8, −100.2	175.4, −121.9	174.7, 174.7	178.8, −118.6	177.8, −121.4
3a	∠E–A–E	102.2	96.9	96.7	99.9	97.3
	∠C–E–A–E	98.9, −89.7	105.8, 94.9	105.3, −95.4	105.1, −92.0	104.9, −93.5

[a] $[Et_4N]^+$. [b] $[Ph_4P]^+$. [c] $[Ph_4As]^+$. [d] Two Sn–S bonds.

bond asymmetry than S_4 (Table 4). Any explanation involving the anomeric effect, which would require different degrees of back-bonding to different A–E bonds, seems inconsistent with the invariant nature of this bond length for any given A, E pair within a molecule, as noted by others.[13]

Across all the data in Tables 1–3, excluding the two compounds of approximate C_2 symmetry, the ∠E–A–E essentially fall into three categories. The narrowest ∠E–A–E are *ca.* 100° and all occur when the R–E–A–E–R unit adopts the *trans*, *trans* [*t*, *t* (or *ap*, *ap* in Klyne and Prelog notation)] conformation.

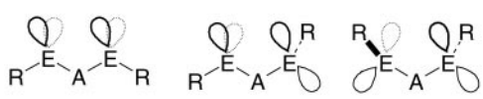

The *t*, *t* combination is only found in $A(ER)_4$ species which adopt D_2 symmetry.

Intermediate ∠E–A–E fall in the range 104–109° and are associated with the *trans*, *gauche* [*t*, *g* (*ap*, *sc*)] pair of conformations. This is a more common combination as it occurs in both S_4 and D_2 symmetries. The largest ∠E–A–E are 111–117° and are for the *g*, *g* (*sc*, *sc*) conformations which are also common to both symmetries. This trend is readily explained by considering the relative orientations of lone pairs across the 1,3-E–A–E moiety. In effect, the lone pairs can be considered to have smaller radial extensions than the bond pairs, thus, for electrons around the 1,3-atoms in an E–A–E moiety, the *compressibility* of the ∠E–A–E depends on which electrons are eclipsed and follows the sequence lp/lp > lp/bp > bp/bp. The three observed conformations for R–E–A–E–R have either 2 pairs of eclipsed lone pairs (*t*, *t*), one lp/lp and one lp/bp eclipsed combination (*t*, *g*), or two lp/bp eclipsed pairs (*g*, *g*), exactly mirroring the trend of increasing ∠E–A–E. Note that the third eclipsed pair in each case (R/R, R/lp, lp/lp) point away from each other and do not affect the ∠E–A–E. This approach is entirely consistent with the LCP model, in which the differences in E···E contacts have been explained in terms of ligand close-packing by the fact that the E has a non-cylindrical electron density distribution as a result of the presence of two lone electron pairs, which makes the effective ligand radius, and hence E···E, a function of orientation.[13]

The situation is less clearly defined for the two selenates of C_2 symmetry (Table 3). For $(2,4,6\text{-}Me_3C_6H_2Se)_4Ge$ both steric crowding of the ligands and/or the presence of weak, intermolecular Se···Se contacts impose additional distortions on the germanium coordination sphere. $(PhSe)_4Sn$ (second conformation) does not suffer these complications and is the only species fully assessed in this paper. Unlike the related species of D_2 or S_4 symmetry, **2c** contains more staggered 1,3 interactions, as seen in the alternate view:

Table 6 Structural data for $[(RS)_4Ga]^-$

Conformation	CODE Symmetry	$[Ga(SEt)_4]^-$ [a] DOMTOO S_4	$[Ga(SPr^i)_4]^-$ [b] GOXHIK D_2	$[Ga(SPh)_4]^-$ [c] DOMTUU D_2
	S···S(short)	3.694 (4)	3.401, 3.496	3.453, 3.509
	S···S(long)	3.706 (2)	3.786, 3.802 3.831, 3.872	3.745, 3.781 3.794, 3.816
t, *t* (*ap*, *ap*)	∠S–Ga–S		97.1	100.3
	∠C–S–Ga–S		−177.4, 161.0	−180.0, −171.8
	∠S–Ga–S		100.9	101.5
	∠C–S–Ga–S		179.6, 173.2	−175.4, 167.9
t, *g* (*ap*, *sc*)	∠S–Ga–S	109.3 (4)		
	∠C–S–Ga–S	164.8, 75.0		
	∠S–Ga–S			
	∠C–S–Ga–S			
g, *g* (*sc*, *sc*)	∠S–Ga–S	109.8 (2)	113.1	112.0
	∠C–S–Ga–S	−44.9, −44.9	62.3, 45.9	−68.9, −58.5
	∠S–Ga–S		114.0	114.2
	∠C–S–Ga–S		57.4, 35.7	51.8, 44.2
	∠S–Ga–S		114.3	114.5
	∠C–S–Ga–S		−79.7, −64.0	−64.6, −51.9
	∠S–Ga–S		118.2	115.0
	∠C–S–Ga–S		−55.7, −55.3	63.5, 56.8

[a] $[^iPr_4N]^+$. [b] $[^iPr_2NH_2]^+$. [c] $[Et_4N]^+$.

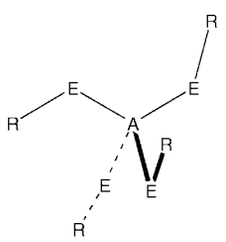

(**2c**)

In the C_2 arrangement, the distinction between "short" and "long" E···E contacts is far less marked than in S_4, as is the degree of angular distortion (Tables 3 and 4).

Table 5 contains data for the anions $[A(ER)_3]^-$, which have approximate C_s symmetry (**3**). All show distortions which lead to two short and one long E···E accompanied by two narrow (87.6–92.8°) and one wider ∠E–A–E (96.7–102.2°). These angles relate to one of two idealised conformations (**3a**, **3b**). **3a** has an eclipsed 1,3 arrangement which brings one lp/lp and one bp/bp into opposition (the remaining pair of lone pairs pointing away from each other), while **3b** is staggered but brings three lone pair sites into close proximity. The narrower ∠E–A–E are associated with the latter conformation, which seems to allow closer approach of atoms by virtue of the restricted size of the lone pairs in much the same way the *t*, *t* conformation does for $A(ER)_4$.

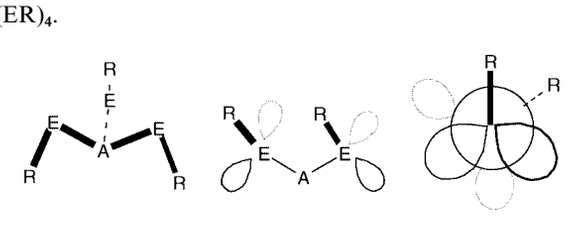

The relationship between ∠E–A–E and the torsion angle ∠C–E–A–E is general, as indicated by examination of the data for the series $[(RS)_4Ga]^-$ (R = Et,[27] ^iPr,[28] Ph [27]) which are isoelectronic with the neutral group 14 series discussed above (Table 6). Two compounds (R = ^iPr, Et) are of approximate D_2 symmetry in which the two narrowest ∠S–Ga–S (*ca.* 100°) are associated with the *t*, *t* C–S–Ga–S conformations, while the four wider angles (*ca.* 114°) correspond to the analogous *g*, *g* conformations. The anion $[(EtS)_4Ga]^-$ is of S_4 symmetry and is unique in being almost perfectly symmetrical with regard to ∠E–A–E, which are all *ca.* 109°. The four angles of 109.3° can be classified as *t*, *g*, in keeping with other $(RE)_4A$ compounds, while the two marginally wider angles (109.8°) are closest to *g*, *g* C–S–Ga–S conformations, though well removed from ideal torsional angles (−44.9, −44.9°). Further examples to which the analysis can be applied are $Mo(SBu^t)_4$ [D_2: ∠S–Mo–S 95.6, conformation *t*, *t*; 116.8, *g*, *g*; 116.9°, *g*, *g*][29] and three examples of $(RS)_2Sn(S_2CNEt_2)_2$ [R = Ph, Cy, CH_2CF_3], which we have discussed elsewhere.[30]

The question of the validity of a LCP model for *semi-ionic* compounds such as those analysed here requires an analysis of the intramolecular E···E non-bonding interactions across a range of compounds and coordination numbers. If the molecular geometry is dictated by ligands which approach to a characteristic close contact, the length of this contact should be fixed across a range of compounds, as has been noted in relatively ionic systems.[12] The majority of data available for a single $A(ER)_4$ system is for $C(OR)_4$, which have been assessed by others.[12,13] The O···O(short) and O···O(long) separations are each remarkably consistent, averaging 2.20 and 2.33 Å, respectively (Table 4). The same pattern emerges from the more limited data for other species. For $Sn(SR)_4$ there are three examples for which S···S(short/long) are 3.79 and 4.04 Å, while there are two examples each for $C(SR)_4$ [S···S(short/long): 2.94, 3.04 Å], $Ge(SeR)_4$ [Se···Se(short/long): 3.79, 3.96 Å] and $Sn(SeR)_4$ [Se···Se(short/long): 4.04, 4.18 Å]. These values seem to be valid, as they can be cross-correlated with related systems. For example, $Ph_2Si(OPh)_2$ (DADKIC) has O···O of 2.730 Å, which is consistent with the longer range for O···O for the sole example of $Si(OR)_4$ (2.72 Å). In addition, the data for $Ph_2Si(OPh)_2$ correspond to an open ∠O–Si–O (112.5°) and a *g*, *g* (*sc*, *sc*) conformation for C–O–Si–O–C (torsion angles −66.8, −59.2°), all entirely consistent with the analysis presented earlier. Two examples are available for comparison with $Sn(SR)_4$: $Ph_2Sn(SPh)_2$ (LESSUX) and $Me_2Sn(SC_{10}H_{10})_2$ (RULFOT). Both have S···S (3.966, 3.953 Å)

Table 7 AM1/DFT optimised geometries for $Sn(SR)_4$ and related species

Conformation	Symmetry	$(PhS)_4Sn$ [a] S_4	$(^tBuS)_4Sn$ [a] S_4	$(^tBuS)_4Mo$ (expt.) D_2	$(^tBuS)_4Mo$ [b] D_2 (calc.) [c]
	A–S	2.42 (4)	2.40 (4)	2.235 (4)	2.268, 2.271 2.272, 2.274
	S···S(short)	3.88 (4)	3.81 (4)	3.310 (2)	3.402, 3.414
	S···S(long)	4.10 (2)	4.16 (2)	3.807 (2), 3.809 (2)	3.860, 3.867 3.820, 3.858
t, *t* (*ap*, *ap*)	∠S–A–S			95.6 (2)	97.1
	∠C–S–A–S			178.4, 178.4	178.7, 178.6
	∠S–A–S				97.4
	∠C–S–A–S				179.8, 175.9
t, *g* (*ap*, *sc*)	∠S–A–S	106.4	104.6		
	∠C–S–A–S	178.3, −55.1	164.3, −37.6		
	∠S–A–S	106.5	104.6		
	∠C–S–A–S	−178.0, 54.4	−164.3, 37.9		
	∠S–A–S	106.5	104.6		
	∠C–S–A–S	54.1, −178.9	164.5, −37.7		
	∠S–A–S	106.6	104.7		
	∠C–S–A–S	−54.1, 178.2	−164.4, 37.7		
g, *g* (*sc*, *sc*)	∠S–A–S	115.5	119.6	116.8 (2)	114.7
	∠C–S–A–S	−63.8, −63.7	79.1, 78.9	54.5, 54.5	55.5, 52.0
	∠S–A–S	115.6	119.7	116.9	116.2
	∠C–S–A–S	62.9, 64.0	−79.0, −78.8	−57.7, −57.7	56.2, 54.2
	∠S–A–S				116.2
	∠C–S–A–S				−60.1, −59.4
	∠S–A–S				116.7
	∠C–S–A–S				−57.5, −57.3

[a] AM1. [b] DFT. [c] Approximate D_2 symmetry.

consistent with the longer value for $Sn(SR)_4$ (4.04 Å), and again both have *g*, *g* (*sc*, *sc*) conformations (LESSUX: ∠S–Sn–S 110.8°, torsion angles −84.5, −68.0°; RULFOT: 109.9, 85.0, 79.7°) and open ∠S–Sn–S.

It is interesting to compare data for $Sn(SR)_4$ with that for the anion $[Sn(SPh)_3]^-$ which has approximate C_s symmetry (**3**; Table 5). The S···S(short/long) intramolecular contacts for the anion are very close for two examples with different cations $[Ph_4P^+, Ph_4As^+]$ [18] and are each *ca.* 0.2 Å shorter than the corresponding distances for $Sn(SR)_4$. Similar differences in E···E bond lengths of *ca.* 0.2 Å apply to the other pairs of $A(ER)_4$/$[A(ER)_3]^-$ groups (Table 4). In LCP terms, this is readily explained in terms of differences in the A(IV)–E *vs.* A(II)–E bond polarities. The change from A^{4+} to A^{2+} will reduce the polarity of the A(δ+)–E(δ−) bond, thereby allowing closer approach of E(δ−)···E(δ−) in compounds of the lower oxidation state.

Molecular orbital considerations. Semi-empirical AM1 [31] full geometrical optimizations have been carried out on $Sn(SR)_4$ (R = ^{t}Bu, Cy, Ph) by using the Spartan 5.0 package of programs;[32] parallel DFT calculations produce essentially the same results. In order to check the reliability of the trends observed at this level, a BP86 density functional investigation (with non-local corrections introduced in a perturbative manner) (coded in Spartan as pBP86-) of the model $Sn(SH)_4$ system has been also undertaken.[33,34]

In each AM1 experiment, the structure has been modelled starting from an arbitrary orientation of the Sn–S–R units and the Sn–S bonds rotated systematically to afford a range of conformers and associated energies. For R = ^{t}Bu, Ph the geometry associated with the minimum energy structure is in good agreement with the crystallographic data. While the calculated Sn–S(Ph) bond is longer than observed by *ca.* 0.03 Å, other intramolecular bond lengths, angles and torsion angles faithfully replicate the observed structures. Importantly, the structure predicted in both cases has approximate S_4 symmetry, with four narrow and two wide ∠S–Sn–C (Table 7). The angular distortions inherent in these systems are therefore integral to its nature and are not a consequence of crystal packing, as is often suggested.

In contrast, modelling the D_2 structure of $Sn(SCy)_4$ proved more difficult for reasons which are apparent in a related analysis of the model species $Sn(SH)_4$. For this latter case, a starting structure of D_2 conformation was adopted with two ∠S–Sn–S of 90° and four ∠S–Sn–S of 120°. The two narrow angles were allowed to open by equal amounts in a systematic manner, while the remaining ∠S–Sn–S and torsion angles were allowed to respond freely to achieve a minimum energy; the resultant energy profile is shown in Fig. 4(a). The structure adopted by $Sn(SCy)_4$ in the solid state is accurately reproduced at the inflection point, at which the ∠S–Sn–S are 98 (2 angles) and 114° (4 angles). However, attempts to optimise the geometry at this point resulted in a change to an S_4 conformation of lower energy. The energy difference between the two conformations for $Sn(SH)_4$ is calculated to be *ca.* 6.5 kJ mol^{-1}, which is in keeping with other work on $C(OH)_4$.[10] It would seem reasonable that, at least in the tin system, D_2 does not represent an energy well but an unstable intermediate with respect to S_4. It is apparent from Tables 1–3 that D_2 is less common than S_4, and for the systems analysed in this paper, in addition to $Sn(SCy)_4$, is observed only for certain $C(OR)_4$ species, where the short C–O bond may present steric clashes in conformations central to conformer interconversion.[10] In other $A(ER)_4$ systems, the longer A–E bonds may render the interconversion process more facile, so its adoption by $Sn(SCy)_4$ is curious. Space filling models (Fig. 5) suggest that D_2 is a markedly more compact structure than S_4 and that when modelled as an S_4 structure, $Sn(SCy)_4$ displays a much more open structure. By adopting the flatter D_2 structure, $Sn(SCy)_4$ can pack efficiently in a layer arrangement [Fig. 6(a)], whilst $Sn(SBu^t)_4$, with its more open S_4 conformation, forms an interpenetrating lattice [Fig. 6(b)]. It is

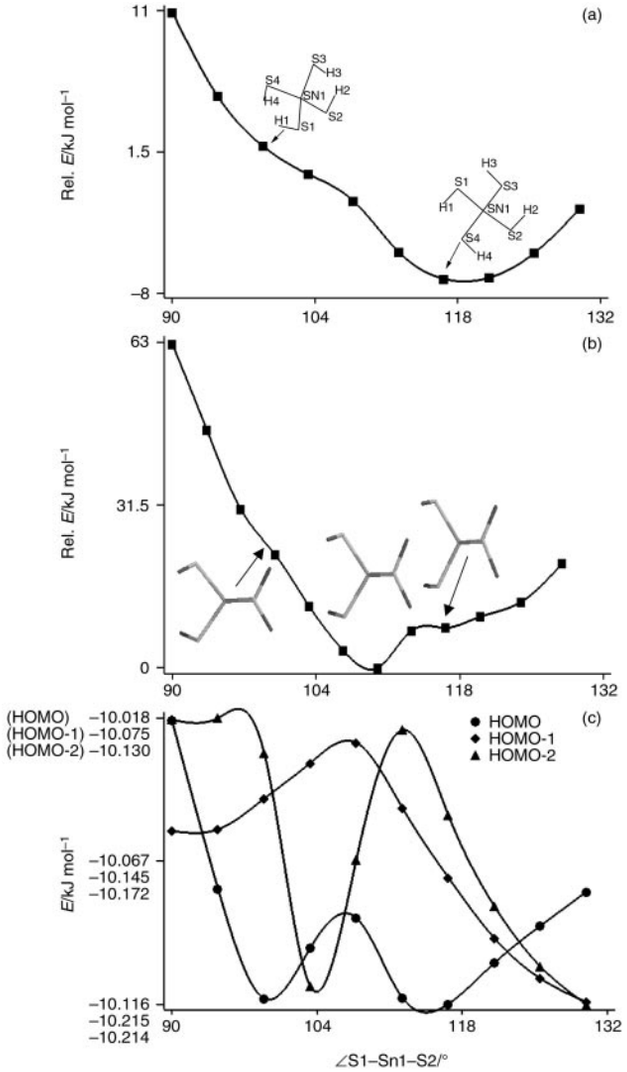

Fig. 4 (a) Variation in the total energy of $Sn(SH)_4$ with ∠S1–Sn–S2 (AM1). The inflection point corresponds to D_2 symmetry while the energy minimum corresponds to S_4. (b) Variation of the total energy of $Sn(SMe)_4$ (the methyl groups attached to S3 and S4 are oriented up and down and those bound to S1 and S2 are oriented inward and outward, respectively) (DFT). (c) Variation in the energies of HOMO (●), HOMO-1 (◆) and HOMO-2 (▲) for $Sn(SH)_4$ as a function of ∠S1–Sn–S2. Energies scales on the *y*-axis correspond to the three MOs in descending order.

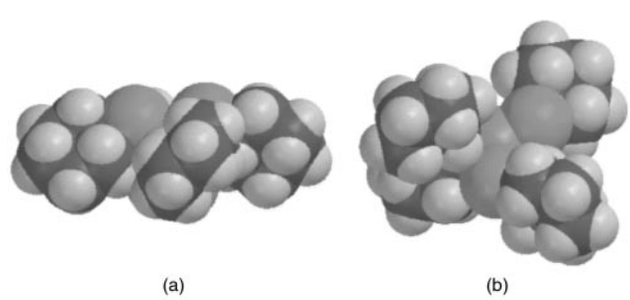

Fig. 5 Space filling models of (a) $Sn(SCy)_4$ D_2 and (b) $Sn(SCy)_4$ S_4.

plausible, therefore, that it is crystal packing effects which favour D_2 over S_4 symmetry in the case of $Sn(SCy)_4$.

The geometry associated with the energy minimum in Fig. 4(a) is of S_4 symmetry and contains ∠S–Sn–S of 106 (4 angles) and 117° (2 angles), again consistent with the solid-state structures of $Sn(SR)_4$ (R = ^{t}Bu, Ph) and the AM1 models of these two compounds (Table 7).

In order to check the validity of the $Sn(SH)_4$ model we repeated the DFT/DN* constrained optimizations at the pBB level for $Sn(SMe)_4$ starting from a C_1 symmetry. Fig. 4(b) shows that the DFT analysis broadly follows that provided by the AM1 and does not depend on the symmetry of the starting point. The D_2 conformation is seen as an inflection point rather than an energy minimum, while the commonly observed S_4 arrangement with two wide angles also appears as an emerging minumim at ∠S–Sn–S 118°. What is new in this figure is the emergence of another local minimum on the overall potential energy surface, corresponding to a more symmetrical distribution of angles, which is not revealed in the AM1 survey presented here. Surprisingly, we are aware of only one species which adopts this arrangement, $[Ga(SEt)_4]^-$ (Table 6).

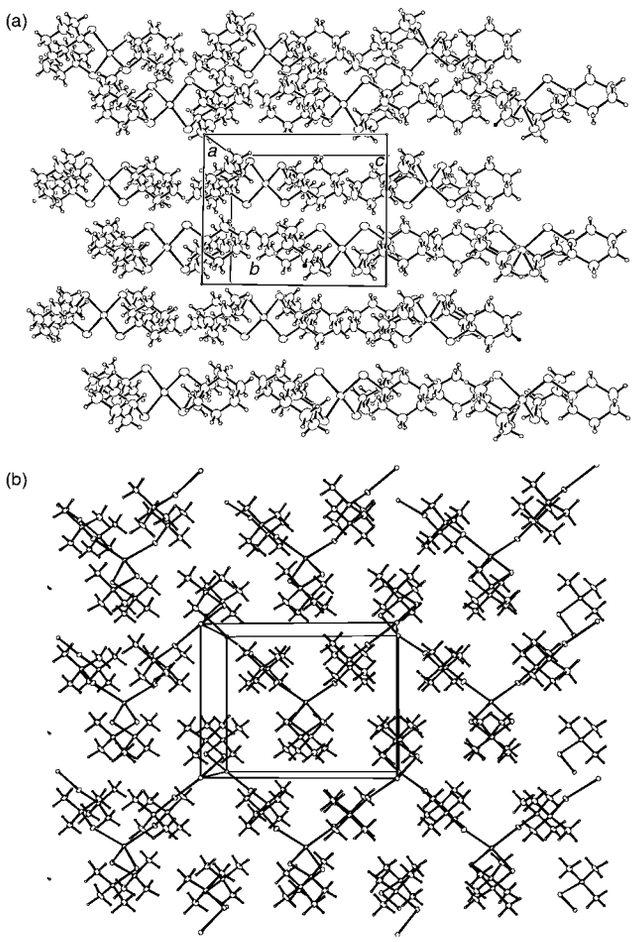

Fig. 6 Unit cell plots of (a) $Sn(SCy)_4$ and (b) $Sn(SBu^t)_4$.

What is not readily apparent in either D_2 or S_4 arrangement is why $A(ER)_4$ should adopt conformations where the ∠E–A–E deviate markedly from 109°28′ at all, rather than more symmetrical geometries; only the anion $[Ga(SEt)_4]^-$ of the structures surveyed herein (Table 6) has been found to adopt a relatively regular metal coordination sphere and even here the torsion angles are consistent with an S_4 assignment. A possible explanation can be found by considering the three HOMOs (HOMO, HOMO-1, HOMO-2) for $Sn(SH)_4$, which, not surprisingly, are associated with the p-orbitals on each sulfur (the lone pairs). Fig. 4(c) shows the energy variation in the three HOMOs, which parallel the total energy variation shown in Fig. 4(a). Fig. 7 shows two views of each of the three HOMOs corresponding to (a) the starting D_2 geometry, (b) the D_2 geometry at the energy inflection point and (c) the S_4 geometry at the overall energy minimum. As the narrow S1–Sn–S2, S3–Sn–S4 angles in D_2 open from 90°, the energies of the HOMO and HOMO-2 fall [Fig. 4(c)] as the anti-bonding interactions across these angles are relieved by p-orbital twisting. In contrast, the energy of HOMO-1 increases as the angles open, primarily because twisting of p-orbitals now reduces the bonding inter-

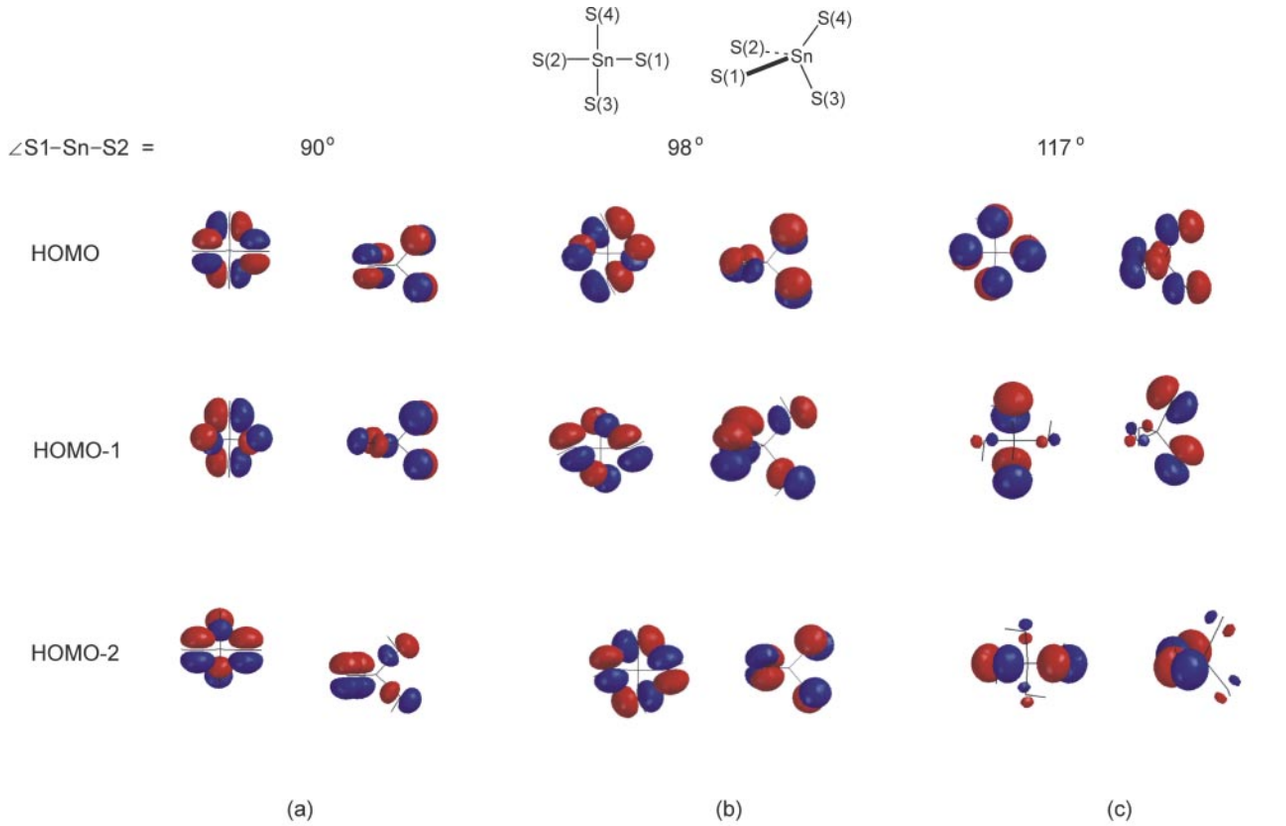

Fig. 7 Pictorial representations of HOMO, HOMO-1 and HOMO-2 for $Sn(SH)_4$ at ∠S1–Sn–S2 = (a) 90, (b) 98 and (c) 117°. The two views of each MO are in the orientations given for (b).

action between S3/S4. The two opposing effects result in the inflection point corresponding to the minimum D_2 energy when ∠S–Sn–S is *ca.* 98°. As these S1–Sn–S2, S3–Sn–S4 angles continue to open, the conformation switches to S_4 and the angles optimise at *ca.* 118°, again as a result of two opposing factors. Firstly, the HOMO is already at a local energy minimum as a result of maximum bonding overlap across S1/S2 and S3/S4, which decreases as the p-orbitals rotate on further widening of their respective S–Sn–S angles. Conversely, the HOMO-1 and HOMO-2 contain essentially one anti-bonding pair of p-orbitals each and therefore favour opening of each of the S–Sn–S angles.

To have an estimate of the overall S···S bond order we used Gaussian 94[35] (installed at the Computational Center for Quantum Chemistry, Athens, GA, USA) with the 3-21G* basis set as well as with the DZVP polarized DFT orbitals basis set and performed single point calculations at the optimum geometries provided by Spartan 5.1.‡ The net S···S bond order from a Mulliken population analysis is essentially zero, and varies from −0.037 when ∠S1–Sn–S2 is 93° to −0.013 at 116°.

While the above analysis goes a long way to rationalising the variations in S–Sn–S angle from the ideal 109°28′ to both greater and smaller values, the reason why thermal decomposition of $Sn(SR)_4$ affords Sn_3O_4, by way of Sn(0), remains open. There is clearly no net S···S bond inherent in $Sn(SR)_4$ precursors, though in both S_4 and D_2 geometries there are bonding combinations based on the lone electron pairs which would promote the formation of S–S bonds and the elimination of RSSR from $Sn(SR)_4$. We therefore speculate that these bonding interactions are ultimately sufficient to determine the outcome of the decomposition pathway.

However, this analysis requires careful application, as it is known the other $M(SBu^t)_4$ (M = Ti, Mo)[36,37] have been used as precursors for the deposition of MS_2. We have carried out DFT calculations for $Mo(SBu^t)_4$, which correctly predict that a D_2 conformation and singlet electronic structure is of lowest energy and also accurately replicate the geometric data of the molybdenum thiolate.[29] Six of the highest MOs are shown in Fig. 8 and, as with $Sn(SH)_4$, are associated with the lone pair orbitals on sulfur. With respect to S···S interactions, HOMO is bonding, HOMO-1 antibonding, HOMO-2,3 net weakly bonding and HOMO-4 weakly antibonding. In summary, there is again no overall drive for S–S bond formation. Furthermore, several of these MOs include contributions from d-orbitals on molybdenum, a feature which is absent in the tin thiolate analysis: HOMO is Mo–S antibonding, HOMO-4 (along with a symmetry related HOMO-6) is strongly σ-bonding, while HOMO-7 is strongly π-bonding. The combined effect of these interactions would be to strengthen the Mo–S bond and thus enables deposition of MoS_2 by effectively promoting C–S bond cleavage at the expense of Mo–S rupture and elimination of RSSR.

Conclusions

The structural distortions in iso-electronic species of empirical formula $A(ER)_4$ can be rationalised in terms of the conformations of the C–E–A–E fragments. The angle E–A–E increases as the C–E–A–E changes from *t*, *t* to *t*, *g* to *g*, *g*, and is consistent with other ligand close packing (LCP) analyses. These distortions are not due to packing effects, as they can be accurately modelled by AM1/DFT calculations based on isolated molecules. Moreover, these calculations reveal significant E···E

‡ Basis sets were obtained from the Extensible Computational Chemistry Environment Basis Set Database, Version 4/22/01, as developed and distributed by the Molecular Science Computing Facility, Environmental and Molecular Sciences Laboratory which is part of the Pacific Northwest Laboratory, P.O. Box 999, Richland, WA 99352, USA, and funded by the U.S. Department of Energy. The Pacific Northwest Laboratory is a multi-program laboratory operated by Battelle Memorial Institute for the U.S. Department of Energy under contract DE-AC06–76RLO 1830. Contact David Feller or Karen Schuchardt for further information.

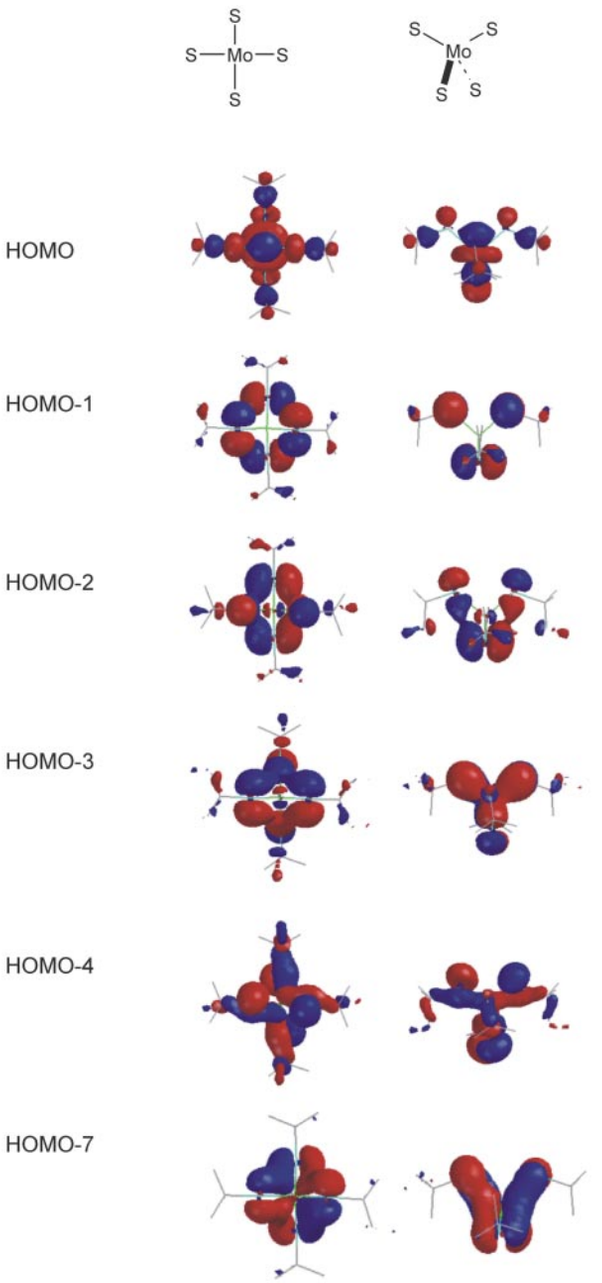

Fig. 8 Pictorial representations of HOMO, HOMO-1, HOMO-2, HOMO-3, HOMO-4 and HOMO-7 for $Mo(SBu^t)_4$ (calculated D_2 geometry).

interactions involving the HOMOs, which are based on the p-orbitals (lone pairs) on E. This offers a rationale as to why certain main group species such as $Sn(SR)_4$ do not decompose to tin sulfides but instead form Sn_3O_4, probably *via* a Sn(0) intermediate. Conversely, transition metal thiolates such as $Mo(SR)_4$, which do decompose to MS_2, have additional S(p)–Mo(d) interactions which strengthen the M–S bond.

Experimental

Infrared spectra were recorded from hexachlorobutadiene mulls between KBr plates using a Nicolet 510P FT-IR spectrophotometer, and elemental analyses were performed using a Carlo-Erba Strumentazione E.A. model 1106 microanalyser operating at 500 °C. ^{1}H and ^{13}C NMR spectra were recorded on a Jeol JNM-GX270 FT spectrometer and ^{119}Sn NMR spectra were recorded on a Jeol JNM-EX400 FT machine, all using saturated $CDCl_3$ solutions, unless otherwise indicated. Details of our Mössbauer spectrometer and related procedures are given elsewhere.[38] Dry solvents were obtained by distillation under inert atmosphere from the following drying agents: sodium–benzophenone (toluene, ether, THF), magnesium (MeOH), sodium (hexane), CaH_2 (MeCN). Standard Schlenk techniques were used throughout. Starting materials were commercially obtained and used without further purification.

Synthesis

$(C_6H_{11}S)_4Sn$. To a solution of cyclohexylthiol (4.2 ml, 34.6 mmol) in dry degassed toluene (100 ml) was added n-butyllithium in hexanes (1.6 M; 22 ml, 25.2 mmol) under dry N_2. A white precipitate ($C_6H_{11}SLi$) formed immediately, which was stirred at room temperature for 20 min. After this time, $SnCl_4$ (1.0 ml, 8.55 mmol) was added and the reaction mixture refluxed for 3 h. Upon cooling to room temperature, the white precipitate (LiCl) was removed by filtration, leaving a colourless solution. Removal of the toluene *in vacuo* left a sticky white solid, which was recrystallised from toluene to give $(C_6H_{11}S)_4Sn$ (3.82 g, 77%) as colourless crystals, m.p. 54.5–55 °C. Found (calc. for $C_{24}H_{44}S_4Sn$): C, 49.8 (49.7); H, 7.76 (7.67)%. ^{1}H NMR: δ 2.06–1.20 (m, 10 H, CH_2), 3.21 (m, 1 H, CH). ^{13}C NMR: δ 43.3, 38.2, 26.4, 25.3. ^{119}Sn NMR: δ 109.2. Mössbauer: IS = 1.31, QS = 0, Γ = 1.15 mms^{-1}. IR spectrum identical to that reported earlier.[17]

$(^tBuS)_4Sn$. The compound was prepared by an analogous method to that for $Sn(SCy)_4$.[14] Found (calc. for $C_{16}H_{36}S_4Sn$): C, 39.6 (40.4); H, 7.40 (7.67)%. ^{1}H NMR: δ 1.61 (s, CH_3). ^{13}C NMR: δ 36.2 (CH_3), 49.5 (CCH_3). ^{119}Sn NMR: δ 24.3. Mössbauer: IS = 0.93, QS = 0.63, Γ = 1.04 mms^{-1}.

$[Ph_4P][(PhS)_3Sn]$. $SnCl_2$ (2.00 g, 10.5 mmol) was dissolved in dry, degassed methanol (20 ml) and PhSNa (4.18 g, 31.7 mmol), also dissolved in methanol (20 ml), added. The resulting solution, containing a yellow precipitate, was warmed to 70 °C and $[Ph_4P]Br$ (4.42 g, 10.6 mmol) dissolved in methanol (50 ml) added. Stirring was continued for 30 min, during which time a voluminous yellow precipitate formed. The precipitate was extracted into MeCN (100 ml) with warming; cooling the extract yielded the title compound as pale yellow crystals (6.40 g, 77%), m.p. 146 °C. Found (calc. for $C_{42}H_{35}PS_3Sn$): C, 63.6 (64.2), H, 4.48 (4.49)%. Mössbauer: IS = 2.88, QS = 1.38, Γ = 0.88 mms^{-1}.

Crystallography

Experimental data relating to all three structure determinations are summarised in Table 8. All three data sets were collected on an Enraf Nonius CAD-4 diffractometer; data were corrected for Lorentz and polarization effects, and structure refinement was full-matrix least-squares on F^2. The solution of the structures and their refinement used SHELX86[39] and SHELX93[40] software, respectively; drawings were produced using ORTEX.[41]

For $Sn(SBu^t)_4$, all atoms were allowed to vibrate anisotropically in the final least squares cycles. Hydrogen atoms were included at calculated positions where relevant. The asymmetric unit (Fig. 1) consists of one quarter of the molecule, where the central Sn atom is located on a special position with crystallographic $\bar{4}$ symmetry.

For $Sn(SCy)_4$, the asymmetric unit (Fig. 2) was found to consist of one quarter of the molecule with the central tin atom situated on a $\bar{4}$ rotation axis. In the final least squares cycles, all atoms were allowed to vibrate anisotropically; hydrogen atoms were included at calculated positions where relevant.

For $[Ph_4P][(PhS)_3Sn]$, data were also corrected for absorption. In the final least squares cycles, all atoms were allowed to vibrate anisotropically. Hydrogen atoms were included at calculated positions where relevant. The asymmetric unit is shown in Fig. 3.

CCDC reference numbers 155165–155167.

See http://www.rsc.org/suppdata/dt/b0/b010157p/ for crystallographic data in CIF or other electronic format.

Table 8 Crystal data and structure refinement for (^{t}BuS)$_4$Sn, Sn(SCy)$_4$ and [Ph$_4$P][(PhS)$_3$Sn]

	$Sn(SBu^t)_4$	$Sn(SCy)_4$	$[Ph_4P][(PhS)_3Sn]$
Empirical formula	$C_{16}H_{36}S_4Sn$	$C_{24}H_{44}S_4Sn$	$C_{42}H_{35}PS_3Sn$
Formula weight	475.38	579.52	785.54
Temperature/K	293(2)	293(2)	293(2)
Crystal system	Tetragonal	Tetragonal	Monoclinic
Space group	$P\bar{4}2_1c$	$P4_2/n$	$P2_1/c$
Unit cell dimensions,			
a/Å	11.305(3)	11.888(1)	10.706(1)
b/Å	11.305(3)	11.888(1)	17.420(2)
c/Å	9.273(3)	10.221(1)	20.170(2)
β/Å			104.72(1)
Volume/Å^3	1185.1(6)	1444.5(2)	3638.2(6)
Z	2	2	4
μ(Mo-Kα)/mm^{-1}	1.425	1.183	0.948
Crystal size/mm	0.2 × 0.2 × 0.2	0.2 × 0.2 × 0.2	0.15 × 0.2 × 0.2
Reflections collected	1904	2388	7098
Independent reflections	896 [R(int) = 0.0296]	1135 [R(int) = 0.0377]	6385 [R(int) = 0.0087]
Final R indices [$I > 2\sigma(I)$]	$R_1 = 0.0297$	$R_1 = 0.0396$	$R_1 = 0.0258$
	$wR_2 = 0.0720$	$wR_2 = 0.0852$	$wR_2 = 0.0851$
R indices (all data)	$R_1 = 0.0582$	$R_1 = 0.0615$	$R_1 = 0.0390$
	$wR_2 = 0.1040$	$wR_2 = 0.0940$	$wR_2 = 0.0943$

Acknowledgements

We thank the EPSRC for funding and NATO for the award of a travel grant (to K. C. M) which initiated the collaboration between Bath and Cluj. We also wish to acknowledge the use of the EPSRC's Chemical Database Service at Daresbury.[42]

References

1 L. S. Price, I. P. Parkin, T. G. Hibbert and K. C. Molloy, *Adv. Mater.*, 1998, **4**, 222.
2 L. S. Price, I. P. Parkin, A. M. E. Hardy, R. J. H. Clark, T. G. Hibbert and K. C. Molloy, *Chem. Mater.*, 1999, **11**, 1792.
3 I. P. Parkin, L. S. Price, A. M. E. Hardy, R. J. H. Clark, T. G. Hibbert and K. C. Molloy, *J. Phys. IV*, 1999, **9**, Pr8.
4 L. S. Price, I. P. Parkin, M. N. Field, A. M. E. Hardy, R. J. H. Clark, T. G. Hibbert and K. C. Molloy, *J. Mater. Chem.*, 2000, **10**, 527.
5 T. G. Hibbert, M. F. Mahon, K. C. Molloy, I. P. Parkin and L. S. Price, *J. Mater. Chem.*, 2001, **11**, 469.
6 G. Barone, T. G. Hibbert, M. F. Mahon, K. C. Molloy, L. S. Price, I. P. Parkin, A. M. E. Hardy and M. N. Field, *J. Mater. Chem.*, 2001, **11**, 464.
7 G. N. Schrauzer, R. K. Chadha, C. Zhang and H. K. Reddy, *Chem. Ber.*, 1993, **126**, 2367.
8 L. C. Damude, P. A. W. Dean, V. Manivannan, R. S. Srivastava and J. J. Vittal, *Can. J. Chem.*, 1990, **68**, 1323.
9 E. Block, G. Ofori-Okai, H. Kang, J. Wu and J. Zubieta, *Inorg. Chim. Acta*, 1991, **190**, 5.
10 N. Narasimhamurthy, H. Manohar, A. G. Samuelson and J. Chandrasekhar, *J. Am. Chem. Soc.*, 1990, **112**, 2937.
11 D. G. Gorenstein and D. Kar, *J. Am. Chem. Soc.*, 1977, **99**, 672.
12 R. J. Gillespie and E. A. Robinson, *Adv. Mol. Struct. Res.*, 1998, **4**, 1.
13 R. J. Gillespie, I. Bytheway and E. A. Robinson, *Inorg. Chem.*, 1998, **37**, 2811.
14 H. J. Backer and J. Kramer, *Rec. Trav. Chim.*, 1934, **53**, 916.
15 H. J. Backer and J. Kramer, *Rec. Trav. Chim.*, 1934, **53**, 1101.
16 R. C. Poller and J. N. R. Ruddick, *J. Chem. Soc., Dalton Trans.*, 1974, 146.
17 H. J. Backer and J. Kramer, *Rec. Trav. Chim.*, 1933, **52**, 437.
18 P. A. W. Dean, J. J. Vittal and N. C. Payne, *Can. J. Chem.*, 1985, **63**, 394.
19 K. Kato, *Acta Crystallogr., Sect. B*, 1972, **28**, 606.
20 R. K. Shibao, N. L. Keder and E. Eckert, *Inorg. Chem.*, 1990, **29**, 4163.
21 M. J. Hampden-Smith, T. A. Wark, A. L. Rheingold and J. C. Huffman, *Can. J. Chem.*, 1990, **69**, 121.
22 D. H. R. Barton and H. Dadoun, *New J. Chem.*, 1982, **6**, 53.
23 H. J. Gysling and H. R. Luss, *Organometallics*, 1989, **8**, 363.
24 I. G. Dance, *Polyhedron*, 1986, **5**, 1037.
25 F. C. Mulhoff, H. J. Geise and E. J. M. v. Schaick, *J. Mol. Struct.*, 1973, **20**, 393.
26 B. Kersting and B. Krebs, *Inorg. Chem.*, 1994, **33**, 3886.
27 L. E. Maelia and S. A. Koch, *Inorg. Chem.*, 1986, **25**, 1896.
28 S. Suh, J. H. Hardesty, T. A. Albright and D. M. Hoffman, *Inorg. Chem.*, 1999, **38**, 1627.
29 S. Otsuka, M. Kamata, K. Hirotsu and T. Higuchi, *J. Am. Chem. Soc.*, 1981, **103**, 3011.
30 T. G. Hibbert, A. T. Kana, M. F. Mahon, K. C. Molloy, I. P. Parkin and L. S. Price, submitted for publication.
31 M. J. S. Dewar, E. G. Zoebisch, E. F. Healy and J. J. P. Stewart, *J. Am. Chem. Soc.*, 1985, **107**, 3902.
32 Spartan version 5, Wavefunction Inc., Irvine, CA, USA.
33 A. D. Becke, *Phys. Rev.*, 1986, **33**, 8822.
34 A. D. Becke, *Phys. Rev.*, 1988, **38**, 3089.
35 M. J. Frisch, G. W. Trucks, H. B. Schlegel, P. M. W. Gill, B. G. Johnson, M. A. Robb, J. R. Cheeseman, T. Keith, G. E. Petersson, J. A. Montgomery, K. Raghavachari, M. A. Al-Laham, V. G. Zakrzewski, J. V. Ortiz, J. B. Foresman, J. Cioslowski, B. B. Stefanov, A. Nanayakkara, M. Challacombe, C. Y. Peng, P. Y. Ayala, W. Chen, M. W. Wong, J. L. Andres, E. S. Replogle, R. Gomperts, R. L. Martin, D. J. Fox, J. S. Binkley, D. J. Defrees, J. Baker, J. P. Stewart, M. Head-Gordon, C. Gonzales and J. A. Pople, Gaussian 94, Gaussian Inc., Pittsburgh, PA, 1994.
36 J. Cheon and G. S. Girolami, *Mater. Res. Soc. Symp. Proc.*, 1993, N1.5/Y1.5.
37 J. Cheon, J. E. Gozum and G. S. Girolami, *Chem. Mater.*, 1997, **9**, 1847.
38 K. C. Molloy, T. G. Purcell, K. Quill and I. Nowell, *J. Organomet. Chem.*, 1984, **267**, 237.
39 G. M. Sheldrick, SHELX86S, Computer Program for Crystal Structure Determination, University of Göttingen, Germany, 1986.
40 G. M. Sheldrick, SHELX93, Computer Program for Crystal Structure Refinement, University of Göttingen, Germany, 1993.
41 P. McArdle, *J. Appl. Crystallogr.*, 1995, **28**, 65.
42 D. A. Fletcher, R. F. McMeeking and D. Parkin, *J. Chem. Inf. Comput. Sci.*, 1996, **36**, 746.